Fuzzy Fusion Techniques for Linear Features Detection in Multitemporal SAR Images

Jocelyn Chanussot, Gilles Mauris, and Patrick Lambert

Abstract—**This paper is concerned with the automatic detection of linear features in SAR satellite data, with application to road network extraction. After a directional prefiltering step, a morphological line detector is presented. To improve the detection performances, the results obtained on multitemporal data are fused. Different fusion strategies involving different fusion operators are then presented. Since extensions of classical set union and intersection do not lead to satisfactory results (the corresponding operators are either too indulgent or too severe), the first strategy consists of fusing the data using a compromise operator. The second strategy consists of fusing the results computed with two operators that have opposite properties, in order to obtain a final intermediate result. Thanks to the wide range of properties they provide, fuzzy operators are used to test and compare these two fusion strategies on real ERS-1 multitemporal data.**

Index Terms— **Data fusion, fuzzy operators, linear features extraction, mathematical morphology, nonlinear filtering, SAR images, road detection.**

I. Introduction

SINCE THE first Earth-viewing spaceborne synthetic aperture radar (SAR) was put into orbit in 1978, numerous radar sensors have been launched (Radarsat, ERS-1 & 2, J-ERS [1]). This success can be partly explained by the good resolution of the obtained images, reached thanks to the synthetic aperture. But, the main point is the ability of the used electromagnetic waves to pass through the clouds, which partly frees the observations from the atmospheric conditions. As a consequence, the images provided by these satellites are now very useful in many remote sensing applications. This paper focuses on one of these applications: the problem of automatic line detection, with application to road network extraction. This is a problem of great importance. For instance, it can be used for cartographic purpose, for the registration of SAR images to existing maps or to other sensor images. But, due to the noisy speckled nature of radar images, this remains quite a difficult task [2]. In particular, it prevents the classical methods, developed for the visible domain (for SPOT or LANDSAT data for instance) from providing satisfactory results. Therefore, specific methods that can deal with these highly corrupted images have been developed. Nevertheless, even well suited algorithms usually lead to imperfect results. To improve these performances, one way consists of using different images of the same scene, acquired at different dates (multitemporal data). The information provided by each available image are then fused, both to increase the detection probability and to reduce the false alarm rate.

In this framework, the paper is organized as follows.

- The first part of the paper presents the detection algorithm that is applied to each image. This is an automatic method based on a morphological approach, preceded by an adaptive directional filtering.
- In the second part, the detections obtained on each image are fused. The responses to the line detector obtained for each pixel at the different dates, seen as uncertain values of detection, are merged together. Different fusion strategies, involving different fusion operators are presented. Thanks to the wide range of properties they can consider, a special attention is paid to fuzzy fusion operators. Results obtained on real multitemporal ERS-1 PRI amplitude data are presented and discussed. See Fig. 1 for the global processing synopsis.

Note that the two parts of the paper are almost independent. The fusion strategies presented in Part B of Section III could be used to aggregate the results obtained with other line detectors.

II. Part A: Automatic Detection of Linear Features

This part presents the algorithm that is used to automatically extract the linear features in each image. The method is organized in two separate steps.

- First, a prefiltering operator is applied to simultaneously smooth the noise and preserve the anisotropic structures. The used directional filter is presented in the first paragraph.
- The second paragraph presents the morphological extraction method that is performed on the filtered images to detect road-pixels.

A. Directional Prefiltering

Most of the classical noise smoothers are based on an additive model. Since radar images are corrupted, by nature, by a multiplicative noise, called the speckle, specific filters that can deal with this model have been developed to perform optimal noise reduction. But, it turned out that these speckle filters [3]–[6], though statistically optimal in terms of noise reduction, are not necessarily the most suited operators to improve the road detection. Actually, for the addressed problem, the useful information lies in anisotropic structures, and

Manuscript received June 4, 1998, revised November 4, 1998.

The authors are with Laboratoire d'Automatique et de MicroInformatique Industrielle, LAMII/CESALP, Université de Savoie-B.P 806, 74016 Annecy Cedex, France, (e-mail: Jocelyn.Chanussot@univ-savoie.fr; Gilles.Mauris@univ-savoie.fr; Patrick.Lambert@univ-savoie.fr).

Publisher Item Identifier S 0196-2892(99)03445-2.

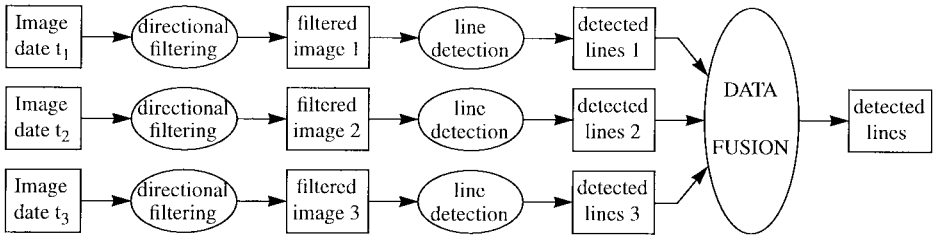

Fig. 1. Global processing synopsis.

the preprocessing operator has to preserve them as well as smooth the noise. Therefore, we used a constrained directional median filter, derived from [7] with adaptive filtering window partitioning.

First, a direction reference map is built. Using the temporal average of the data, the direction associated to each pixel is selected as the most homogeneous direction (according to the range) among all the possible orientations of an 11 pixels long segment shaped filtering window. To get a robust estimation, this direction map is smoothed using a majority vote (the mode) within an 11×11 filtering window. A median filter is then applied on each image separately, using an 11 pixels long segment shaped filtering window, whose direction is set for each pixel by the reference map. This produces a strong noise reduction with a good linear structure preservation. The drawback is the appearance of many 11 pixels long linear artifacts. The size of the filtering window is empiric. It just has to be smaller than the minimum length of the sought structures so that the induced artifacts do not trouble the detection step.

Fig. 2(a) and (b), respectively, present an original ERS-1 PRI amplitude image (a region near Saragosse, in Spain) and the result of the directional filter. The smoothing effect along the linear features is clearly visible, as well as the appearance of the numerous short artifacts.

B. Morphological Extraction

For the extraction step, the model shape and size of the features we are looking for have first to be fixed. We thus decided to characterize the roads in the image as features that are as follows.

- *Locally Rectilinear*: Each road pixel belongs to a segment that is longer than a *minimum* required length l_0. We fixed this minimum length l_0 to 21 pixels (corresponding to approximately 280 meter ground lengths for the processed data, which is a realistic minimum straight line length for typical countryside roads).
- *Thin*: Detected features must not be wider than a maximum width l_1. We decided to seek roads that are up to $l_1 = 3$ pixels wide, which is a typical maximum response width in ERS-1 images for common roads [12].
- *Contrasted*: Roads appear on SAR data as linear features that are either darker or lighter than their surroundings.

Different methods based on edge detectors [12], [17], [18], statistical [15], [16], Markovian [12], [14], or neural [13] approaches have been proposed in the literature for the extraction of linear structures. But, since the features we are looking for are intrinsically characterized by their shape, it seemed natural to us to use morphological operators [8]–[11]. The proposed method is simple and fast [19]. It is unsupervised: there is no need for preselected points or for training images. It is also almost nonparametric (apart from the model dimensions, one single threshold is involved). This is thus a robust and generic approach that can be used over a wide range of images, applications and sensors.

We will now detail the operators used for the detection of **light linear features**. The extension to dark features is straightforward: one just has to use the dual operators (erosion/dilation, opening/closing).

In the following, we will use the classical topographic analogy for the representation of gray-scale images. In this representation, the image is considered as a topographic relief, the numerical value of each pixel determining the corresponding point elevation. With this analogy, light linear features correspond to **elongated and narrow mountains** in a topographic relief. Fig. 3(a) presents a zoom of the small $20*20$ square taken in the original image [white square in Fig. 2(a)] and its corresponding relief. Fig. 3(b) presents the same image after the directional prefiltering. The strong smoothing effect, with preservation of the linear structures is fairly perceptible. But, there nevertheless still remain some parasite structures. Actually, three different types of structures have to be removed, each one violating one of the basic constraints of the model definition.

- We first remove the structures that are **darker** than their surroundings (corresponding to "**valleys**" in the relief). This is done using a morphological closing by reconstruction with a flat square structuring element of size 5 [20]. This operator fills in the nonflat valleys of the image. Furthermore, this is a connected operator: it therefore does not introduce any new discontinuity in the image. Calling I_0 the original filtered image and using classical notations, we obtain the image I_1:

$$I_1 = \overline{\varphi}_5(I_0). \tag{1}$$

  Fig. 3(c) presents the studied portion of I_1 and its corresponding relief representation.
- We then remove **nonlinear (or too short) mountains**, and preserve the others. This is achieved by taking the *supremum* (denoted "$\vee$") of all the possible l_0 long directional openings. It is computed using linear structuring elements successively oriented in every possible direction d_i (40 different directions for a 21 pixels long linear

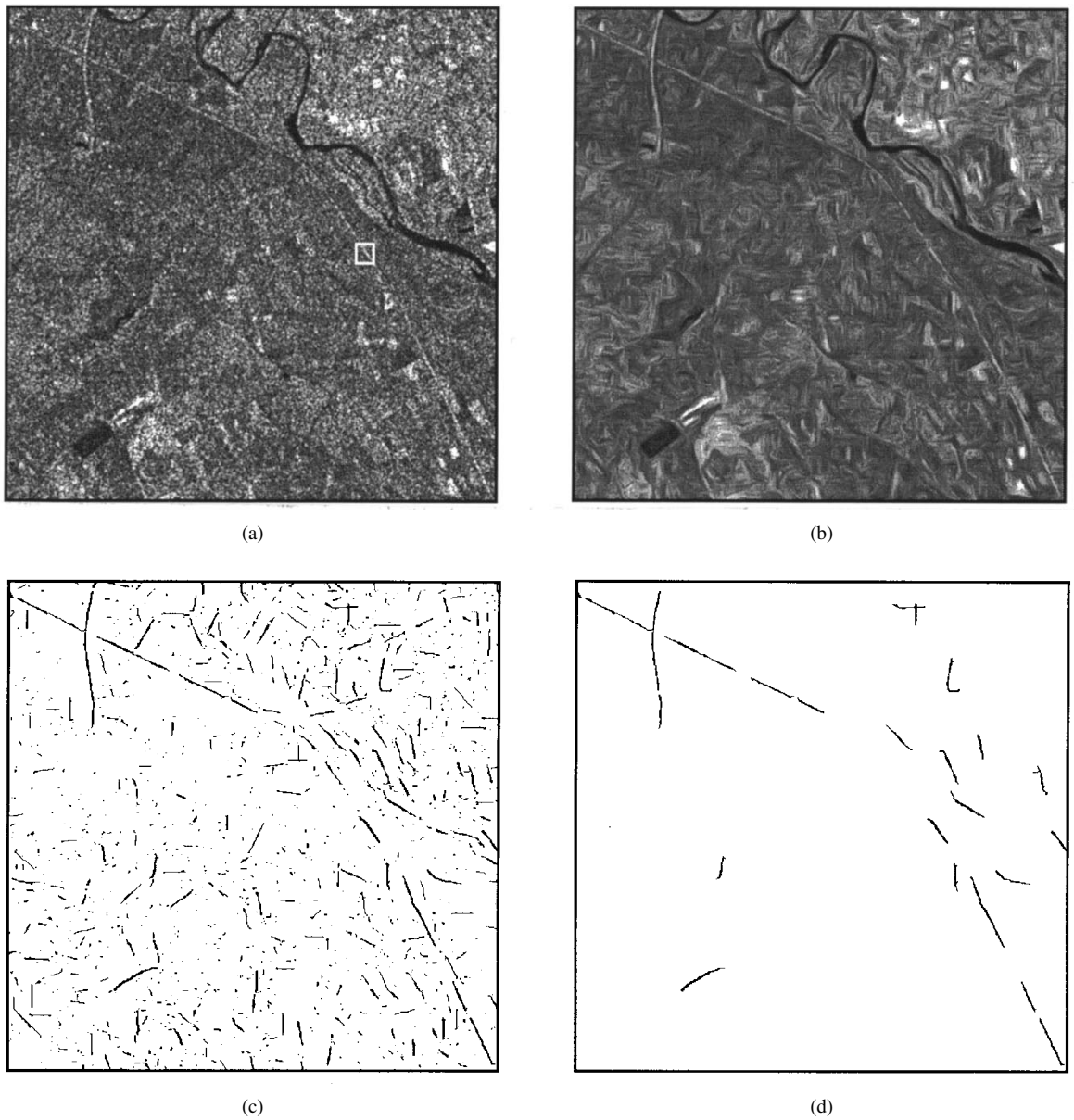

(a) (b) (c) (d)

Fig. 2. Directional filtering of an original SAR image and obtained detection. (a) Original image, (b) directionally filtered image, (c) detection performed on the filtered image, and (d) "cleaned" detection.

structuring element). We obtain the image I_2 defined by

$$I_2 = \vee_{di}\{\gamma_{di}(I_1)\}, \quad \text{with} \quad i \in \{1, \cdots, 40\}. \tag{2}$$

Fig. 3(d) presents the studied portion of I_2 and its corresponding relief representation.

- Since we first used a closing by reconstruction with an 8-connectivity grid, some "isolated" valleys remain that could lead to false detection in the next step. These remaining valleys are now removed with a simple closing using a flat square structuring element of size 5 (without any reconstruction). Behind this operation appears a new constraint: we assume that two different roads will be separated by at least five pixels, which is a realistic assumption (five pixels approximately correspond to 60 m on the ground). We then obtain the image I_3:

$$I_3 = \varphi_5(I_2). \tag{3}$$

Fig. 3(e) presents the studied portion of I_3 and its corresponding relief representation.

- We finally remove the remaining linear mountains, that are actually at least l_0 pixels long, but are **too wide** (more than l_1), and extract the desired structures. The residue between the current image and its opening of size l_1 is calculated (top-hat operator). The only remaining structures are the light features that are up to l_1 pixels wide. Any other pixel is put to zero. We obtain the image I_4 defined as follows:

$$I_4 = I_3 - \gamma_3(I_3). \tag{4}$$

Fig. 3(f) presents the studied portion of I_4 and its corresponding relief representation.

Image I_4 constitutes the response to the line detector. The final binary decision (road pixel or not) is taken by threshold-

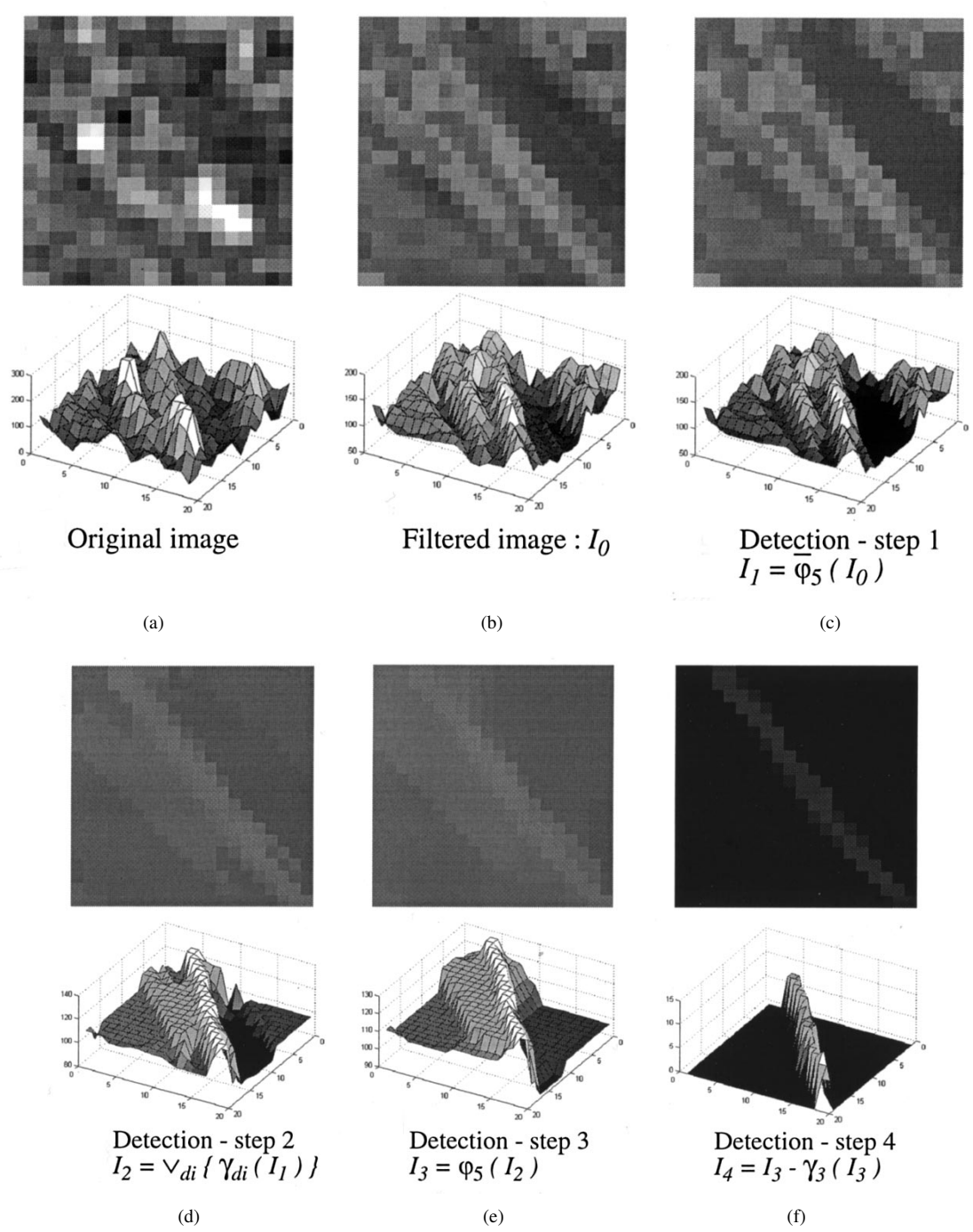

Fig. 3. (a) Part of the original image and (b) the prefiltering and the different steps leading to the extraction (c)–(f) and the corresponding relief representations.

ing it. Fig. 2(c) shows the result of the detection obtained on the original filtered image, with 5 as threshold value. This result can then be "cleaned" by removing the smallest detected segments. Fig. 2(d) presents the result obtained after the removal of the connected components that have a less than 50 pixels area. Nevertheless, apart from the visual quality of the results, this "cleaning" must be used very carefully since all small removed features are not necessarily noisy features. Some of them really belong to the road network and could highly increase the quality of the detection in a following step.

Though quite satisfactory, these results are far from perfect. Some false alarms still remain, and the detection is not exhaustive: roads are disconnectively detected. To improve these performances, a high level post processing step that globally analyzes the image is usually applied. It aims at suppressing the false alarms and at reconnecting the detected segments in order to fully reconstruct the road network. Tupin [12], for instance, recently proposed such a reconnection step based on a markovian approach. Nevertheless, the better the local detection is, the better the final reconnection will be. In this framework, the next part shows how the multitemporal fusion of the marginal detections can improve the local detection performances. This would greatly facilitate the global reconnecting step that could be performed afterwards.

III. Part B: Multitemporal Fusion of the Results

This part presents different approaches to fuse the detection results obtained on the same scene at different dates (these multitemporal data have previously been manually registered). The response of a pixel to the line detector is linearly mapped into [0, 1] and is then considered as a confidence degree in its being part of a potential road. The degrees obtained at the different dates have to be merged. After the fusion, the result is linearly mapped back into [0, 255]. The **final decision** is put off to the end of the processing: the binary thresholding is applied **after** the fusion has been performed. This classically ensures more flexibility: a decision taken on the fused data generally leads to better results than the fusion of the different decisions. In particular, it can better deal with conflictual situations.

Extensions of classical union and intersection set operations are first briefly described in Section I. The corresponding operators are not satisfactory: they are either too severe or too indulgent. As a consequence, we then propose two different fusion strategies to obtain intermediate results: Section II presents different compromise operators, whereas Section III explains how to combine two "extreme" operators in order to build an intermediate one. Fuzzy operators [22]–[27] provide different tools to implement these approaches. Finally, Section IV presents and discusses the results obtained with each operator on real multitemporal amplitude ERS-1 data.

Note that most of the presented fusion rules assume that the data are "independent." Actually, common data are usually favored by the fusion, but if the sources are linked, this increase of trust is misleading. This "independence" is not the statistical independence. It only means that the data are acquired and processed independently. Since the images we process are acquired at different dates, spread over a few months, and since the detection processing is performed on each image separately, it is valid to use these fusion operators. We assume that the roads remain unchanged from one image to another (redundancy of information), whereas the noise (artifacts due to the fields, unfortunate realizations of the noise and s.o.) is assumed to be nonredundant from one image to another. Generally speaking, the fusion aims at exploiting the information redundancy and the nonredundancy of the noise to increase the detection performance and to reduce the false alarm rate.

Notations: In the following, we assume that K sources are available, corresponding to the images of the same scene acquired at K different dates. The response of a pixel from the kth image to the line detector will be denoted x_k and the associated estimated direction will be denoted d_k.

A. Union and Intersection

To extend the notions of set union and set intersection to fuzzy sets, two classes of operators (T-norms and T-conorms) are usually defined [32], [33].

- T-norms generalize the notion of set intersection. A T-norm is defined as an application i: $[0, 1]^2 \rightarrow [0, 1]$ such that:
  - i is commutative, associative and increasing with respect to both variables,
  - 1 is the neutral element: $i(x, 1) = x$.

  A T-norm has always a conjunctive (severe) behavior.
- T-conorms generalize the notion of set union. A T-conorm is defined as an application u: $[0, 1]^2 \rightarrow [0, 1]$ such that:
  - u is commutative, associative, and increasing with respect to both variables,
  - 0 is the neutral element: $u(x, 0) = x$.

  A T-conorm has always a disjunctive (indulgent) behavior.

In the following, we will test the *minimum* operator (5), which is the greatest possible T-norm: the output $x_\wedge$ is computed as the minimum of the K responses.

$$x_\wedge = \min_k \{x_k\} \tag{5}$$

This operator is severe: a pixel will be classified as road pixel if and only if it was classified as road pixel on every image taken separately (if the same threshold value is used, this corresponds to the intersection of the results). As a consequence, such an operator will produce an excellent false alarm rate reduction, but it will provide poor detection performances, though with high confidence level. Using another T-norm will accentuate this effect, suppressing more false alarms, but more detections too.

The logical counterpart of the *min* operator is the indulgent *maximum* operator, which is the smallest possible T-conorm. The corresponding output $x_\vee$ is the *max* of the responses:

$$x_\vee = \max_k \{x_k\}. \tag{6}$$

This operator leads to very good detection performances, since one single response greater than the threshold value is enough to classify a pixel as road pixel (this corresponds to the union of the results). But, as a consequence, the false alarm rate is not reduced; on the contrary, all the false alarms of the K different sources are added. Using another T-conorm will accentuate this effect, providing more detections, but more false alarms too.

Due either to a poor detection or to a dramatic false alarm rate, none of these operators is satisfactory. Thus, the general idea is to find a compromise between a purely conjunctive and a purely disjunctive behavior, trying to take advantage of them both. This can be done using two different approaches: the first one, described in Section II consists of directly using a compromise operator for fusing the data. The second one, described in Section III consists of fusing the results of a conjunctive fusion and of a disjunctive fusion together, in order to get an intermediate global behavior.

B. Compromise Operators

A fusion operator is said to be a compromise (cautious behavior) if it is always included between the *min* and the *max* operators. Different classical classes of fuzzy operators behave in this way.

1) Mean Operators: A mean operator [32]–[34] m is an application m: $[0, 1]^2 \rightarrow [0, 1]$ such that

- $\min(x, y) \leq m(x, y) \leq \max(x, y)$;
- $m \neq \min$ and $m \neq \max$;

- m is commutative and increasing with respect to both variables.

The arithmetical mean x_{mean} of course belongs to this class of operators. It will be tested in the following.

$$x_{mean} = \frac{1}{K} \cdot \sum_{k=1}^{K} x_k. \tag{7}$$

Beyond classical averaging operators, mean operators constitute a very large family that also include OWA operators [29] described in the following (Section II-C) and the fuzzy integrals [35], [36]. The behaviors of these operators proceed from their definition: they always behave like a compromise.

2) Adaptive Quantified Fusion (AQ): The main idea of the adaptive quantified operator proposed by Dubois and Prade [26], [31] is to assume that only j sources, among the K available, are reliable. These j sources are first aggregated with a conjunctive rule (T-norm). But, although the number j is assumed to be given, the reliable sources remain unknown: as a consequence, all the possible fusions of j sources among K are computed, and the results are then aggregated with a disjunctive operator (T-conorm). We obtain the operator x_{AQ} (8):

$$x_{\mathrm{AQ}} = \text{T-conorm}_{J \subset \{1, \ldots, K\}, card(J)=j} \{\text{T-norm}_{k \in J}(x_k)\}. \tag{8}$$

The first difficulty with this method is to estimate the number of reliable sources. Delmotte [28] defines some criteria to determine j automatically according to a cost function. The second difficulty lies in the practical computation of the output: the apparent combinational explosion can be reduced, in some particular cases, as follows.

1) Rank the data increasingly:

$$x_1, x_2, \cdots, x_K \rightarrow x_{(1)} \leq x_{(2)} \leq \cdots \leq x_{(K)}. \tag{9}$$

2) a) if the used T-conorm and T-norm, respectively, correspond to the *max* and to the *min*, the output of the operator turns out to be simply the $(K - j + 1)$ ordered data:

$$x_{\mathrm{AQ}} = x_{(K-j+1)} \tag{10}$$

b) if the used T-norm is the product operator, the output turns out to be the product of the j greatest data:

$$x_{\mathrm{AQ}} = x_{(K-j+1)} . x_{(K-j+2)} \cdots x_{(K)}. \tag{11}$$

Some of these operators also belong to the class of the mean operators. But, if the used T-norm and T-conorm differ from the *min* and the *max*, operators defined by (8) can go beyond the *max* or below the *min*: there is no inclusion between these two families. The key point is that these operators perform a **partial aggregation**: unreliable sources are not taken into account. In the following, we will test one operator from this family: the operator defined by (10). It will then be reported as x_{OWA}, since it also belongs to the family described in the next section.

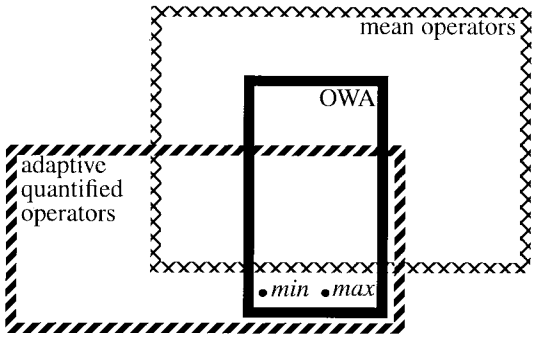

Fig. 4. Partial inclusions between the different presented classes of operators.

3) Order Weighted Averaging Operator: The ranked data as defined by (9) can also lead to another class of compromise fusion operators: the order weighted averaging operators (OWA) [29]. These operators are defined as a linear combination of the ranked input data:

$$x_{\mathrm{OWA}} = \sum_{k=1}^{K} w_k \cdot x_{(k)}. \tag{12}$$

Depending on the weighting vector (w_k), the *min* and *max* operators can be considered as particular cases of OWA operators, as well as the arithmetical mean or even the quantified operator introduced by (10) (if $k = K - j + 1 w_k = 1$, else $w_k = 0$). This particular operator will be tested on real data in the following. It will then be reported as x_{OWA}. Note that, on the contrary, the operator defined by (11) is not an OWA operator: there is no inclusion relation between the OWA and the adaptive quantified operators, though there is a nonempty intersection. On the contrary, apart from the limit cases *min* and *max*, any OWA operator is a mean operator. Fig. 4 summarizes the relations existing between the different classes of operators we presented in this section.

Also note that the OWA operators correspond, with a different semantics, to an important class of nonlinear filters in signal and image processing: the order statistics based L-filters [30]. Ranking the data pushes aberrant values to the extreme positions away. Using suitable weighting vector for the linear combination will allow not to take these values into account. In that sense, these operators also perform partial aggregation.

C. Fusion of Extreme Operators

In order to obtain a fusion that is neither purely conjunctive, nor purely disjunctive, previous paragraph presented different compromise operators. Another strategy consists in first using two "extreme" operators (a conjunctive one and a disjunctive one) and in then combining their results together to provide a globally intermediate result. Section III-A presents a context dependent operator whose behavior is ruled by a conflict measure. Section III-B presents a morphological approach based on geodesic reconstruction.

1) Context Dependent Fuzzy Operator: Used separately, T-norms or T-conorms cannot help for the fusion: we want to simultaneously reduce the false alarm rate and to increase the detection, but T-norms, as the *min* operator, will reduce both detections and false alarms, whereas T-conorms, as the *max*

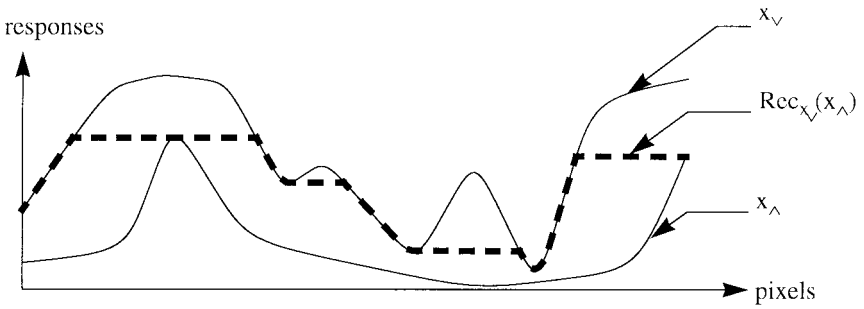

Fig. 5. Geodesic reconstruction of $x_\wedge$ in $x_\vee$

operator, will have the opposite effect. To take advantage of these two opposite properties, we will use a weighted mean of a T-norm i and a T-conorm u ruled by parameter σ (13). As σ ranges from 0 to 1, the resulting operator continuously ranges from a conjunctive to a disjunctive behavior.

$$x_{\mathrm{CD}}(x_1, \cdots, x_K) = \sigma \cdot u(x_1, \cdots, x_K) + (1-\sigma) \cdot i(x_1, \cdots, x_K). \quad (13)$$

In order to take judiciously advantage of both operators, parameter σ has to be adapted to the context of each pixel, leading to an adaptive context dependent (CD) operator [22].

As a consequence, the weights σ and $(1-\sigma)$ are adaptively determined using a compatibility measure [25]. A compatibility relation on a universe Ω is an application σ such that

- $\forall x \in \Omega$, $\sigma(x, x) = 1$: a number is fully compatible with itself;
- $\forall (x, y) \in \Omega^2$, $\sigma(x, y) = \sigma(y, x)$: commutativity;
- For a given x, $\sigma(x, y)$ is a convex fuzzy set.

We want to have the maximum compatibility ($\sigma = 1$: fully compatible sources) when all the sources found the same direction. On the contrary, we want the minimum compatibility ($\sigma = 0$: incompatible sources) when orthogonal estimated directions are found. For a given pixel, we thus defined the compatibility relation between two different images i and j as the absolute value of the cosine between the two directions d_i and d_j selected by the directional opening during the extraction step Section II-B:

$$\sigma(x_i, x_j) = |\cos(d(i), d(j))|. \quad (14)$$

Other monotonous functions respecting the desired conditions could also have been used. Nevertheless, the empiric choice of the cosine is naturally well suited to quantify angular gaps.

To extend this definition to the K sources case, Yager [24] proposed to take the minimum of the compatibilities obtained for every pair of sources. We chose to calculate the product of these compatibilities to be more severe (15).

$$\sigma = \left| \prod_{k,l} \cos(d(k), d(l)) \right|. \quad (15)$$

The operator x_{CD} tested in the following uses this compatibility measure, and takes the *min* operator for the T-norm, and the *max* for the T-conorm. A further improvement consists in using other T-norms and T-conorms in order to induce a reinforcement effect [25]. For instance, the classical operators defined in (16) and their extension to the K sources case (17) can replace the *min* and the *max* in (13):

$$\begin{aligned} u(x_1, x_2) &= x_1 + x_2 - x_1 x_2 \\ i(x_1, x_2) &= x_1 x_2 \end{aligned} \quad (16)$$

$$\begin{aligned} u(x_1, \cdots, x_K) &= \sum_{k=1}^{K} \left\{ (-1)^{k+1} \cdot \sum_{(i_1, \cdots, i_k) \in \{1, \cdots, K\}^k} x_{i_1} \cdots x_{i_k} \right\} \\ i(x_1, \cdots, x_K) &= \prod_{i=1}^{K} x_i \end{aligned} \quad (17)$$

The obtained operator, reported as $x_{\mathrm{CD\_R}}$ in the following, still has a compromise behavior for medium σ values, but the limit cases go respectively beyond the *max* and below the *min*. This results in favoring coherent data and in handicapping incoherent data.

2) Markers and Geodesic Reconstruction: We now propose a morphological approach to fuse a conjunctive operator (for instance, the *min*) with a disjunctive one (for instance the *max*) in order to obtain an intermediate result. Due to the nonredundancy of the noise, the response to the line detector of false alarm pixels is not great in every image. These pixels thus have a small value in the *min* output. As a consequence, since the *min* operator ensures a high confidence degree, its result can be considered as a reference **marker**. To take advantage of the good detection provided by the *max*, the geodesic reconstruction of the *min* in the *max* is computed [20]. This is performed by iterating the geodesic dilation of the *min* under the *max* (18) until idempotence (19).

$$\delta_{geo,\, x_\vee}(x_\wedge) = \inf\{x_\vee, \delta(x_\wedge)\} \quad (18)$$

$$\mathrm{Rec}_{x_\vee}(x_\wedge) = \lim_{n \to \infty} (\delta^n_{geo,\, x_\vee}(x_\wedge)). \quad (19)$$

This defines the following fusion operator, whose output is x_{recons}:

$$x_{recons} = \mathrm{Rec}_{\max_k\{x_k\}}\left(\min_k \{x_k\} \right). \quad (20)$$

This is illustrated by the example presented on Fig. 5 on a monodimensional example ($x_\wedge$ is dilated "horizontally" and is bound by $x_\vee$).

Since the result is necessarily included between the *min* and the *max*, this operator always gives less false alarms than the *max* and more detections than the *min*. The hypothesis induced by such a reconstruction is that any connected part

detected in the *max* that is marked by the *min* will be preserved for the final decision (it is either removed or preserved, but it cannot be cut up into smaller fragments). Thus, the improvement will be optimal when false alarms and good detections are not connected together (otherwise they both are reconstructed), and when the markers provided by the *min* are sufficiently discriminating (false alarms should not be marked) and exhaustive (all roads detected in the *max* should be marked by the *min*).

IV. Results and Comments

Fig. 6 presents the results obtained on real multitemporal ERS-1 PRI amplitude data provided by the IGN (French National Geographic Institute). These are three looks images and the pixel spacing is 12.5 m. For each image, three different acquisitions spread over a few months were available. The detections performed on each of these images are fused using the different operators presented in the previous sections.

- Fig. 6(a) presents three different original images: we sought the **light** linear features in the first two images. We sought the **dark** linear features in the last one.
- Fig. 6(b) and (c) presents the detections obtained, respectively, with the *min* and with the *max* operators. Threshold value for the binary decision is set to 5 for the light roads (first two images) and to 2 for the dark ones that are less contrasted with their surroundings (last image). These values will be kept constant for all the tested operators to allow an objective comparison. The *min* leads to very good false alarm rate reduction, but to extremely poor detection. On the contrary, the *max* leads to excellent detection, but to a dramatic false alarm rate. This justifies the quest for intermediate results.
- Fig 6(d) present the detections obtained with the mean operator (x_{mean}). A "cleaning" that removes all connected components that have a less than 50 pixels area has been applied. Note that the same "cleaning" will be applied with all the other operators. The results are quite good, both in terms of detection improvement and in terms of false alarm reduction. The main roads are almost connectively detected.
- Fig. 6(e) presents the detection obtained with the OWA operator (x_{owa}). Among the three available sources, we assumed that at least two were reliable. The results are more satisfactory in terms of false alarm reduction: almost none of them remain visible. But, the detection is slightly worse: the main roads are disconnectively detected. This could be easily improved by a global post-processing reconnection step.
- Fig. 6(f) presents the results of the geodesic reconstruction of the *min* under the *max* (x_{recons}). As expected, the detection performances are good. In particular, the connection of the detected roads is very good. But some false alarms remain: this is either due to noise features that are connected to the road network, or to a lack of selectivity of the markers provided by the *min*. A solution could be to "clean" the result of the *min* before the reconstruction, another solution could be to use other results, such as x_{owa}, as marker function.
- Fig. 6(g) and (h) presents the results obtained with the adaptive context dependent operator, respectively, without reinforcement effect (x_{CD}) and with reinforcement effect ($x_{\mathrm{CD\_R}}$). Most of the time, the compatibility measure leads to the right weighting between the conjunctive and the disjunctive results. In particular, the detection is quite good. But some false alarms still remain. This is slightly improved by the reinforcement effect [some more noisy features are deleted in Fig. 6(h)].

To choose the most appropriate fusion operator, the user first has to set the cost attached to each false alarm and to each nondetection. The choice is then made depending on the determined tolerated compromise and is application dependent. Nevertheless, with the tested configurations, the reinforced context dependent operator and the geodesic reconstruction provide the best results in terms of detection connectivity. On the contrary, the best false alarm rate reduction is given by the OWA operator.

V. General Conclusion and Perspectives

This paper was concerned with the automatic line detection in satellite radar images, with application to the road network extraction. After a directional prefiltering step, a morphological extraction is performed. Based on a geometrical approach, the proposed line detector does not take explicitly the specific nature of radar data into account and is therefore suboptimal. It is nevertheless useful and interesting since it is simple and fast, unsupervised and almost nonparametric.

To globally improve the detection performances, the results obtained on the same image acquired at different dates (multitemporal data) are fused together. Simple extensions of set union and intersection did not provide satisfactory results: the corresponding operators are either too indulgent or too severe. As a consequence, we proposed two different strategies to obtain an intermediate result. The first approach consisted of directly defining an operator that fuses the data with a compromise behavior. The second approach consisted of combining the results obtained with two extreme operators (a severe and an indulgent one) in order to have a globally intermediate result. Different operators, mostly fuzzy operators, allowed us to implement these two different strategies on real ERS-1 multitemporal amplitude data.

All the presented operators provided interesting compromise results. They all greatly contributed to improve the detection performances. Nevertheless, none of them provided perfect results as they could be obtained by a manual extraction. For instance, false alarms found in mountainous areas (see the top of the second presented image) are not suppressed. But let us recall that the proposed methods only meant at performing the local detection of linear structures. A global reconnecting post-processing that uses high level prior knowledge is usually applied.

Improved implementations of the two proposed strategies are possible. For instance, some improvements could be made in the definition of compromise operators: an operator that simultaneously takes a conflict measure and the reliability of the different sources into account (for instance, an adaptive OWA operator) could lead to better results. Concerning the

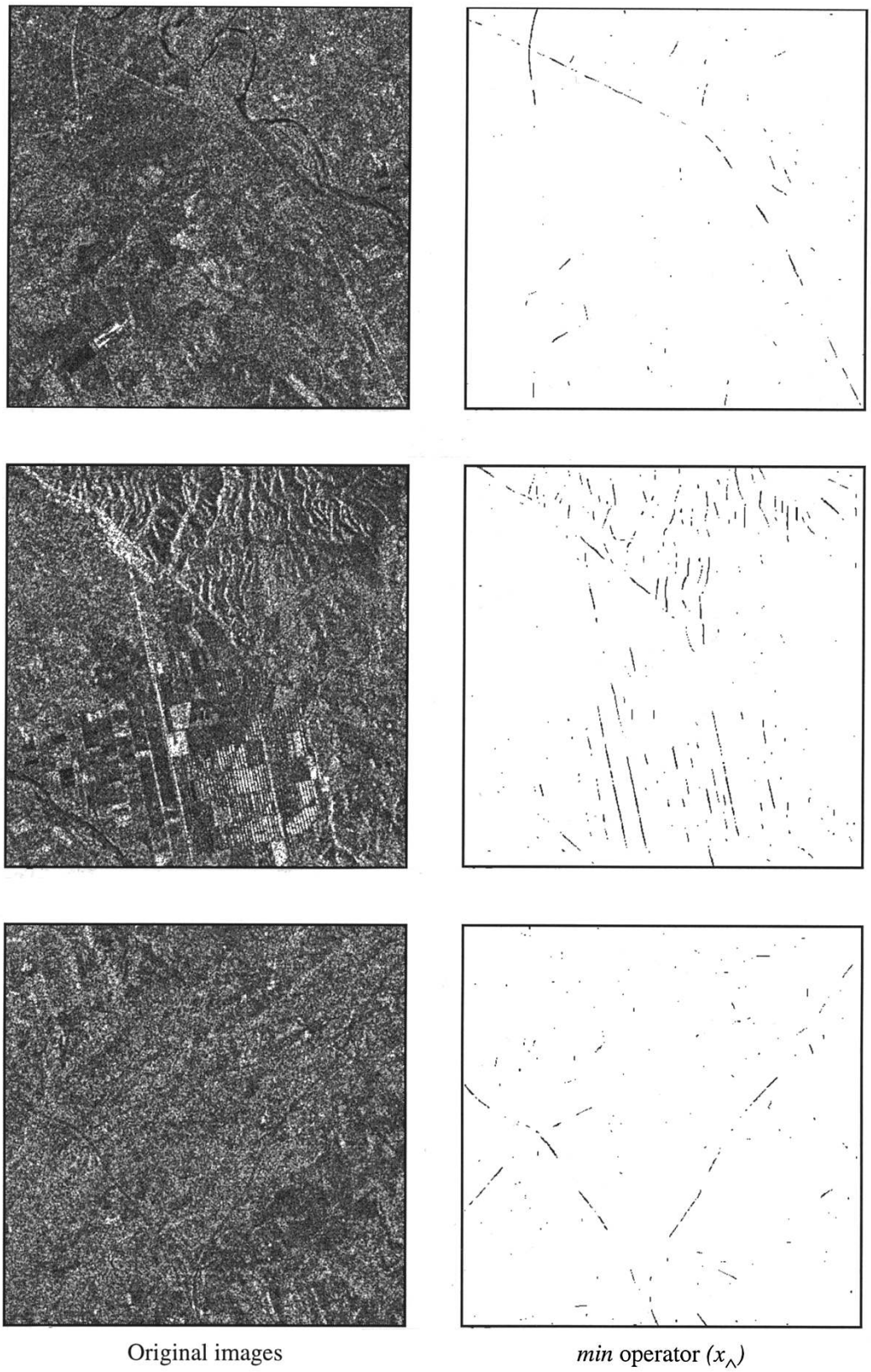

Fig. 6. Detection results with different fusion operators. (a) Original images. (b) min operator $x_\wedge$.

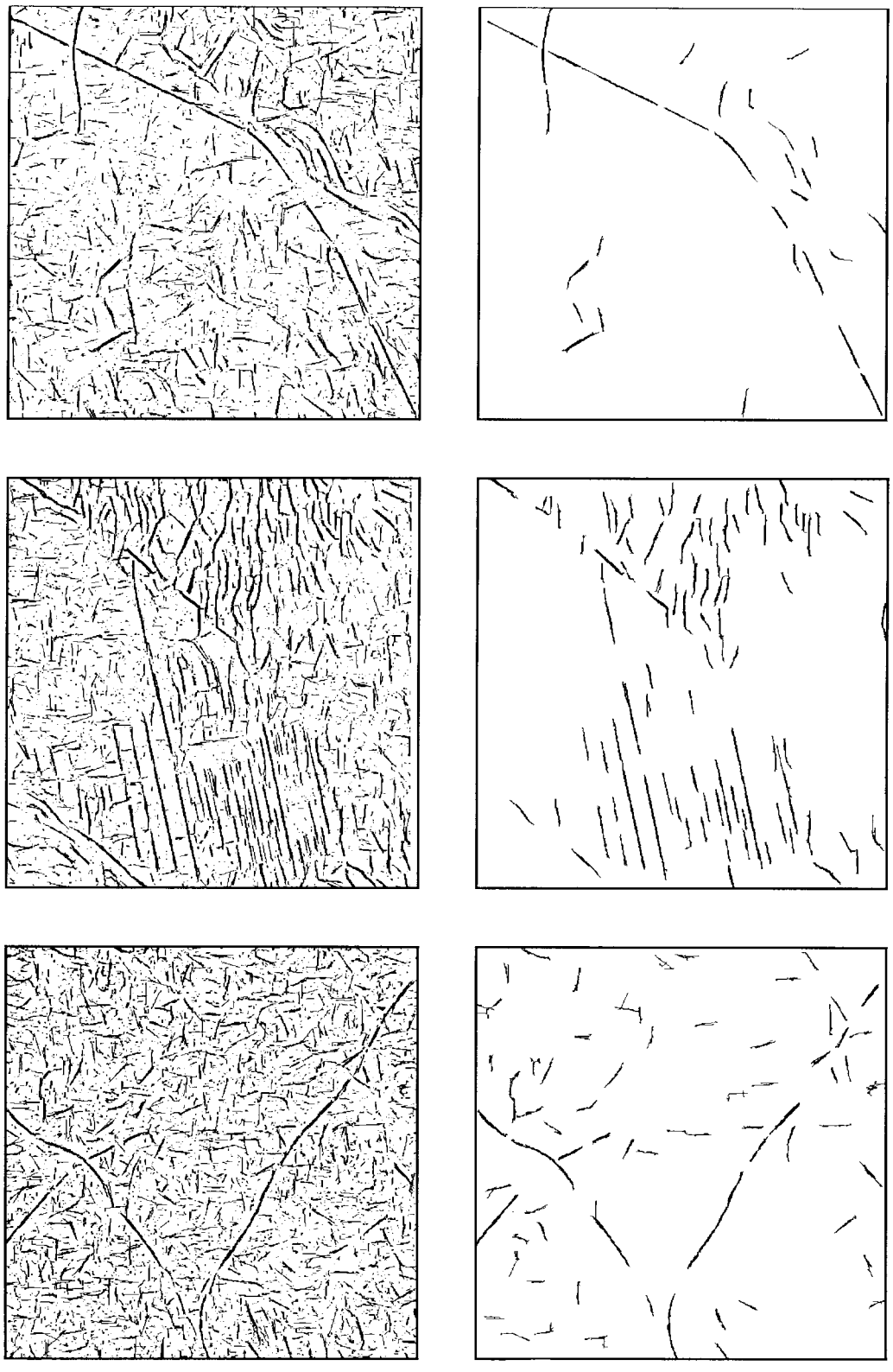

(c) (d)

Fig. 6. (*Continued.*) Detection results with different fusion operators. (c) max operator $x_{\wedge}$. (d) Mean operator (x_{mean}).

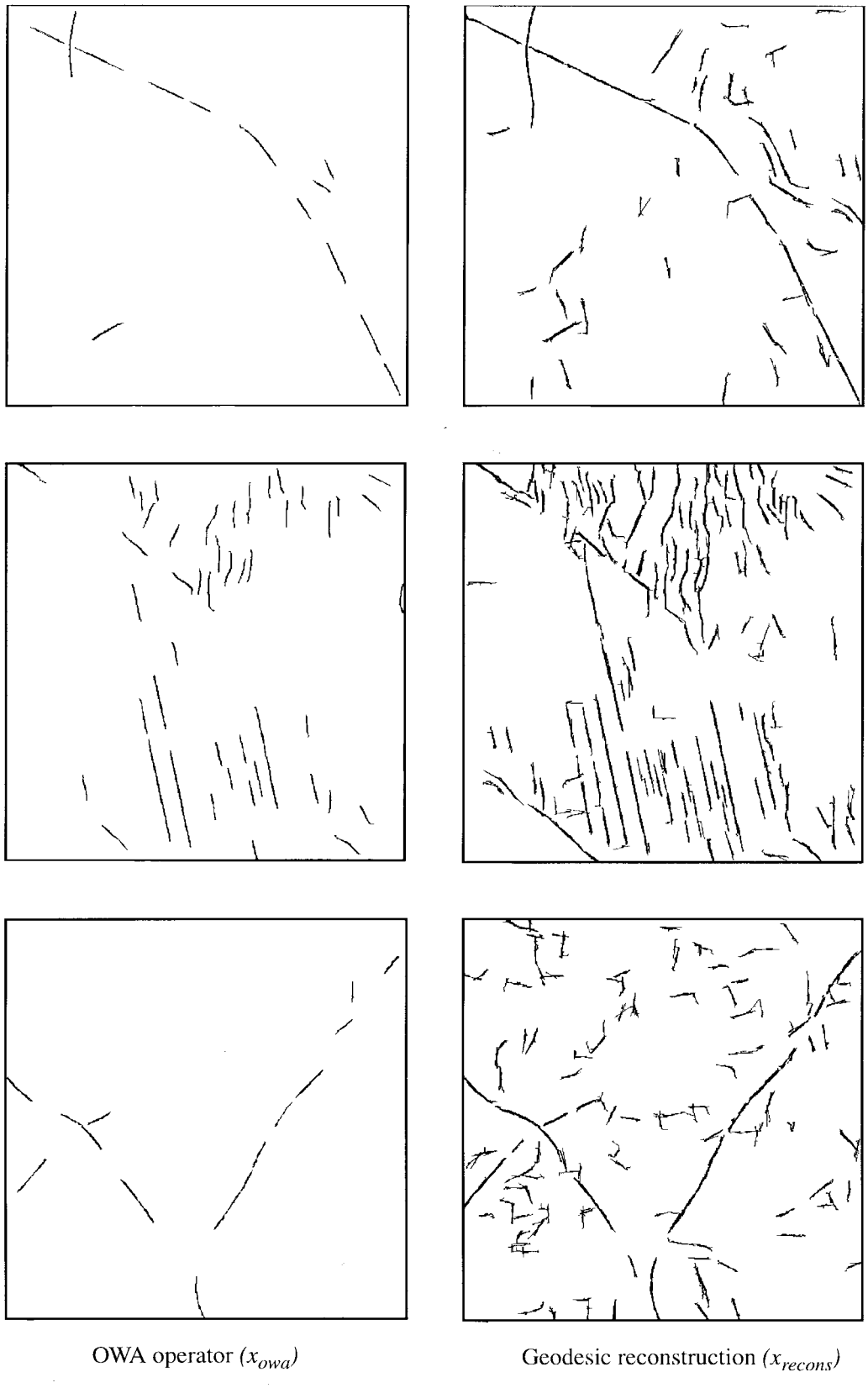

(e) (f)

Fig. 6. (*Continued.*) Detection results with different fusion operators. (e) OWA operator (x_{owa}. (f) Geodesic reconstruction (x_{recons}).

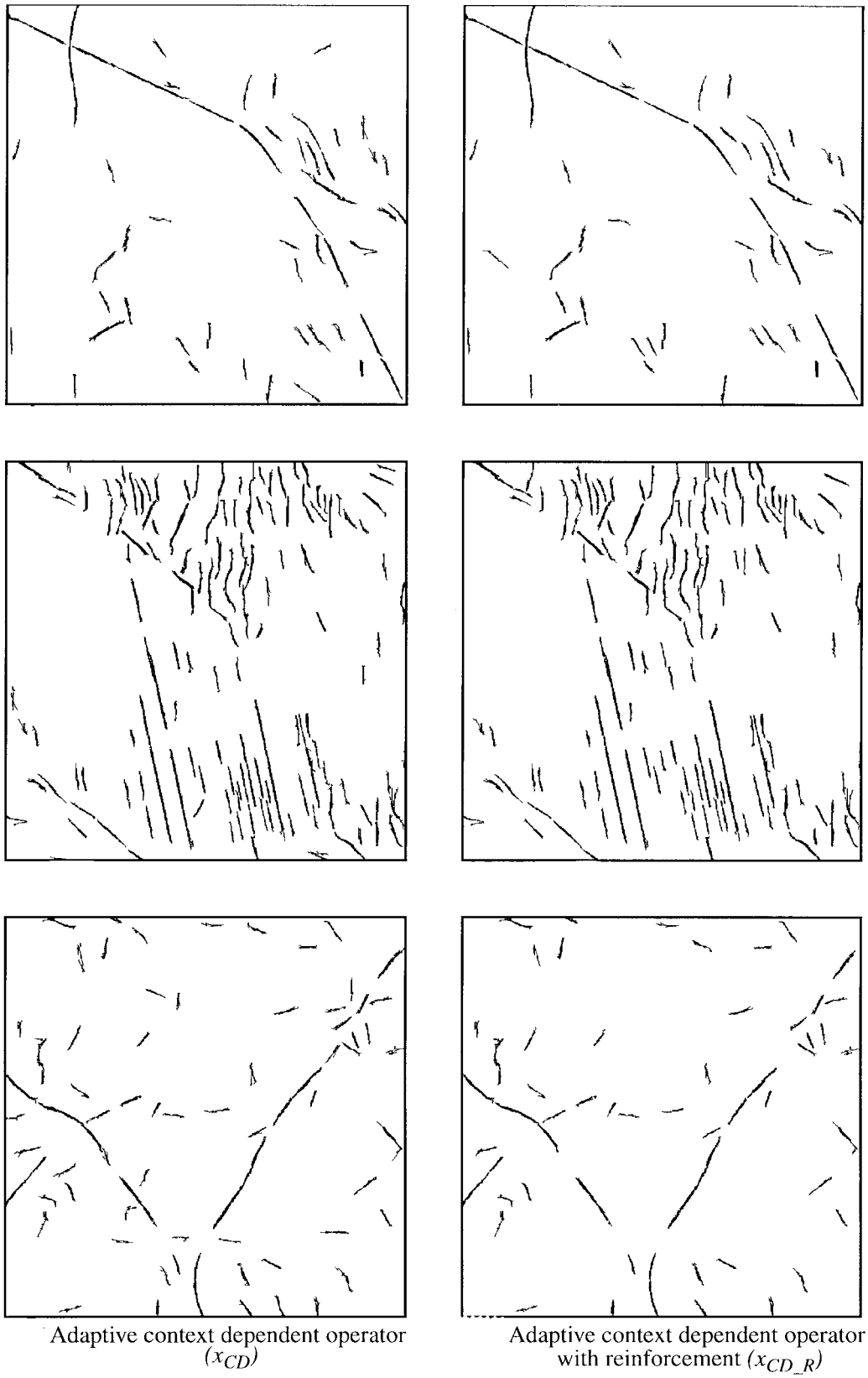

(g) (h)

Fig. 6. (*Continued.*) Detection results with different fusion operators. (g) Adaptive context dependent operator (x_{CD}). (h) Adaptive context dependent operator with reinforcement (X_{CD_R}).

second strategy, another fusion layer consisting of fusing the results of more than two fusion operators could also improve the results.

In order to achieve a better discrimination between the good detections and the false alarms, a key point is the taking into account of the (local) context of each pixel. Therefore, operators that have a constant behavior, though providing an interesting compromise, offer very restricted perspectives. In the same way, operators with variable behavior that only adapts to the values to be fused themselves (such as the associative symmetrical sums [22]) also seem inadequate to discriminate finely between detections and false alarms. In this frame, we believe that the second presented strategy is more promising: the degree of freedom constituted by the way the two (or more ...) chosen fusion operators are combined ensures an optimal flexibility. In particular, taking the context more globally into account (for instance by introducing external complementary information) can be more easily achieved.

For the addressed application, also note that other data could have been used. For instance, whereas we only used amplitude data, Hellwich [21] showed that the coherence images also contain information about linear features that have a width slightly larger than the system resolution. Multisensor data (for instance ERS-1 and JERS-1) could also be used. But, beyond the presented application, this paper principally aimed at presenting different fusion strategies and different classes of fusion operators. These operators could be used in many other remote sensing applications, involving different objectives or different sensors.

REFERENCES

[1] J. Way and E. Atwood Smith, "The evolution of synthetic aperture radar systems and their progression to the EOS SAR," *IEEE Trans. Geosci. Remote Sensing,* vol. 29, pp. 962–985, Nov. 1991.

[2] A. Hendri, S. Quegan, and J. Wood, "The visibility of linear features in SAR images," in *Proc. IEEE Int. Geoscience Remote Sensing Symp.,* 1988, pp. 1517–1520.

[3] J. Bruniquel and A. Lopes, "Analysis and enhancement of multitemporal SAR data," *Proc. SPIE,* vol. 2315, pp. 342–353, 1994.

[4] J. S. Lee, M. Grunes, and S. Mango, "Speckel reduction in multipolarization, multifrequency SAR imagery," *IEEE Trans. Geosci. Remote Sensing,* vol. 29, pp. 535–544, July 1991.

[5] A. Lopes, R. Touzi, and E. Nezry, "Adaptive speckle filter and scene heterogeneity," *IEEE Trans. Geosci. Remote Sensing,* vol. 28, pp. 992–1000, Nov. 1990.

[6] C. Ju and C. Moloney, "An edge-enhanced modified Lee filter for the smoothing of SAR image speckle noise," in *Proc. IEEE Workshop Nonlinear Signal Image Processing,* Mackinac Island, MI, 1997.

[7] P. Zamperoni, "Adaptive rank order filters for image processing based on local anisotropy measures," *Digital Signal Process.,* vol. 2, pp. 174–182, 1992.

[8] J. Serra, *Mathematical Morphology.* London, U.K.: Academic, 1982, vol. 1.

[9] ———, *Mathematical Morphology, Theoretical Advances.* London, U.K.: Academic, 1988, vol. 2.

[10] E. Dougherty, *Mathematical Morphology in Image Processing.* New York: Marcel Dekker, 1993.

[11] H. J. A. M. Heijmans, *Morphological Image Operators.* New York: Academic, 1994.

[12] F. Tupin, H. Maître, J. F. Mangin, J. M. Nicolas, and E. Pechersky, "Detection of linear features in SAR images: Application to road network extraction," *IEEE Trans. Geosci. Remote Sensing,* vol. 36, pp. 434–453, Mar. 1998.

[13] O. Hellwich, "Detection of linear objects in ERS-1 SAR images using neural network technology," in *Proc. IEEE Int. Geoscience Remote Sensing Symp.,* Pasadena, CA, 1994.

[14] O. Hellwich and H. Meyer, "Extracting line features from synthetic aperture radar scenes using a Markov random field model," in *Proc. 3rd IEEE Int. Conf. Image Processing,* Lausanne, Switzerland, vol. 3, pp. 883–886, 1996.

[15] A. Evans, N. Sharp, and E. Hancock, "Noise models for linear feature detection in SAR images," in *Proc. 1st IEEE Int. Conf. Image Processing,* Austin, TX, 1994, vol. 1, pp. 466–470.

[16] R. Samadani and J. Vesecky, "Finding curvilinear features in speckeld images," *IEEE Trans. Geosci. Remote Sensing,* vol. 28, pp. 669–673, July 1990.

[17] M. Adair and B. Guindon, "Statistical edge detection operators for linear feature extraction in SAR images," *Can. J. Remote Sensing,* vol. 16, no. 2, pp. 10–19, 1990.

[18] A. Bovik, "On detecting edges in speckle images," *IEEE Trans. Acoust., Speech, Signal Processing,* vol. 36, pp. 1618–1627, Oct. 1988.

[19] J. Chanussot and P. Lambert, "An application of mathematical morpholohy to road network extraction on SAR images," in *Proc. 4th Int. Symp. Mathematical Morphology Its Applications,* Amsterdam, The Netherlands, 1998, pp. 399–406.

[20] J. Crespo, J. Serra, and R. Schafer, "Theoretical aspects of morphological filters by reconstruction," *Signal Process.,* vol. 47, pp. 201–225, 1985.

[21] O. Hellwich and C. Streck, "Linear structures in SAR Coherence data," in *Proc. IEEE Int. Geoscience Remote Sensing Symposium,* Lincoln, NE, 1996, vol. 1, pp. 330–332.

[22] I. Bloch, "Information combination operators for data fusion: A comparative review with classification," *IEEE Trans. Syst., Man, Cybern. A,* vol. 26, pp. 52–67, Jan. 1996.

[23] R. Yager and D. Filev, *Essentials of Fuzzy Modeling and Control.* New York: Wiley, 1994.

[24] R. Yager, "A general approach to the fusion of imprecise information," *Int. J. Intell. Syst.,* vol. 12, pp. 1–29, 1997.

[25] R. Yager and A. Kelman, "Fusion of fuzzy information with considerations for compatibility, partial aggregation and reinforcement," *Int. J. Approx. Reas.,* vol. 15, pp. 93–122, 1996.

[26] D. Dubois and H. Prade, "Possibility theory and data fusion in poorly informed environments," *IFAC Contr. Eng. Practice,* vol. 2, no. 5, pp. 811–823, 1994.

[27] D. Dubois, H. Prade, and C. Testemale, "Weighted fuzzy pattern matching," *Fuzzy Sets Syst.,* vol. 28, pp. 313–331, 1988.

[28] F. Delmotte and P. Borne, "Modeling of reliability with possibility theory," *IEEE Trans. Syst., Man, Cybern. A,* vol. 28, pp. 78–88, Jan. 1998.

[29] R. Yager, "On ordered weighted averaging aggregation operators in multicriteria decisionmaking," *IEEE Trans. Syst., Man, Cybern.,* vol. 18, pp. 183–190, 1988.

[30] A. Bovik, T. S. Huang, and D. C. Munson, "A generalization of median filtering using linear combinations of order statistics," *IEEE Trans. Acoust., Speech, Signal Processing,* vol. ASSP-31, pp. 1342–1350, 1983.

[31] D. Dubois and H. Prade, "Adaptive combination rules for possibility distributions," in *Proc. EUFIT 2nd Europ. Congr. Intelligent Technics and Soft Computing,* 1994, pp. 48–52.

[32] ———, "A review of fuzzy sets aggregation connectives," *Inform. Sci.,* vol. 36, pp. 85–121, 1985.

[33] R. Yager, "Connectives and quantifiers in fuzzy sets," *Fuzzy Sets Syst.,* vol. 40, pp. 39–75, 1991.

[34] ———, "On mean type aggregation," *IEEE Trans. Syst., Man, Cybern. B,* vol. 26, pp. 209–221, Apr. 1996.

[35] M. Sugeno, "Theory of fuzzy integrals and its applications," Ph.D. dissertation, Tokyo Inst. Technol., Tokyo, Japan, 1974.

[36] M. Grabisch, "On the use of fuzzy integrals as a fuzzy connective," in *Proc. 2nd IEEE Int. Conf. Fuzzy Systems,* San Fransisco, CA, 1993, pp. 213–218.

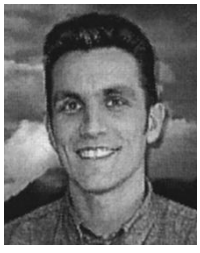

Jocelyn Chanussot graduated in electrical engineering from the Grenoble National Polytechnic Institute (INPG), Grenoble, France, in 1995. He is currently pursuing the Ph.D. degree in the Automatics and Industrial Micro-Computer Science Laboratory (LAMII), Université de Savoie, Annecy, France. His research interests include multicomponent image processing, nonlinear filtering, remote sensing, and data fusion.

Gilles Mauris graduated from the Ecole Normale Superieure de Cachan, France, in 1985. He received the Ph.D. degree in 1992.

He is currently Assistant Professor of Electrical Engineering at the Savoie University (Technological Academic Institute) and works in the Automatics and Industrial Micro-Computer Science Laboratory (LAMII), Annecy, France. His research interests include fuzzy logic, possibility theory, and data aggregation in the instrumentation and measurement area.

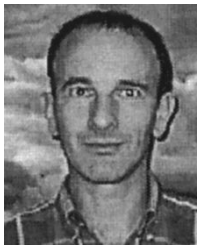

Patrick Lambert graduated in electrical engineering from the Grenoble National Polytechnic Institute (INPG), Grenoble, France, in 1978. He received the Ph.D. degree in signal processing in 1983.

He is currently Assistant Professor of electrical engineering at the Savoie University (Technological Academic Institute) and works in the Automatics and Industrial Micro-Computer Science Laboratory (LAMII), Annecy, France. His research interests include color image representations and segmentations, multicomponent image processing and analysis, data fusion, and fuzzy logic.